arXiv:2107.01214v1 [stat.ML] 2 Jul 2021

Truncated Marginal Neural Ratio Estimation

Benjamin Kurt Miller
University of Amsterdam
b.k.miller@uva.nl

Alex Cole
University of Amsterdam
a.e.cole@uva.nl

Patrick Forré
University of Amsterdam
p.d.forre@uva.nl

Gilles Louppe
University of Liège
g.louppe@uliege.be

Christoph Weniger
University of Amsterdam
c.weniger@uva.nl

Abstract

Parametric stochastic simulators are ubiquitous in science, often featuring high-dimensional input parameters and/or an intractable likelihood. Performing Bayesian parameter inference in this context can be challenging. We present a neural simulator-based inference algorithm which simultaneously offers simulation efficiency and fast empirical posterior testability, which is unique among modern algorithms. Our approach is simulation efficient by simultaneously estimating low-dimensional marginal posteriors instead of the joint posterior and by proposing simulations targeted to an observation of interest via a prior suitably truncated by an indicator function. Furthermore, by estimating a locally amortized posterior our algorithm enables efficient empirical tests of the robustness of the inference results. Such tests are important for sanity-checking inference in real-world applications, which do not feature a known ground truth. We perform experiments on a marginalized version of the simulation-based inference benchmark and two complex and narrow posteriors, highlighting the simulator efficiency of our algorithm as well as the quality of the estimated marginal posteriors. Implementation on GitHub. [1]

1 Introduction

Parametric stochastic simulators are ubiquitous in science [1–3] and using them to solve the Bayesian inverse problem is of general interest. Likelihood-based methods like Markov chain Monte Carlo (MCMC) [4, 5] or nested sampling [6] are applicable when the likelihood is tractable. It is equally common that the likelihood is only implicitly defined by the simulator or is inefficient to compute. For this so-called *likelihood-free* or *simulation-based* inference, the traditional approach is Approximate Bayesian Computation (ABC) [7].

Simulation-based inference (SBI) has been an open research topic for years. Deep learning has accelerated progress in the field [8–11]. Proposed algorithms that learn the likelihood [10] or the posterior [11–13] utilize a density estimator. The likelihood-to-evidence ratio [8] can be learned via a classification-based technique. Refs. [8] and [11] were brought into a unified framework by [14].

High-fidelity simulators often have many parameters and/or an intractable likelihood function, which can make inference notoriously difficult. Practitioners are usually faced with observational data and an expensive stochastic simulator, without access to the ground truth posterior. They want a testably accurate posterior estimate without extreme simulation expense. With existing methods, the practitioner must choose between increased accuracy per simulation or efficient empirical testability. We provide a method which offers both simultaneously with a balance that can be tuned by a hyperparameter. Three attributes contribute to this goal:

[1] Code available at https://github.com/bkmi/tmnre/. Underlying library https://github.com/undark-lab/swyft/.

Preprint. Under review.

Table 1: Comparison of SBI methods, including our proposed TMNRE. See text for details.

Method / Property	Likelihood-based	ABC	NRE	NPE	SNRE	SNPE	**TMNRE**
Targeted inference	✓	•	✗	✗	✓	✓	✓
Simulator efficient *direct* marginals	✗	✓	•	•	✗	✗	✓
(Local) amortization	✗	✗	✓	✓	✗	✗	✓

Targeted inference. Focusing simulations on the parameter regions that are most relevant for the inference problem and target data is more efficient. This is particularly true when most posterior density is concentrated compared to the prior's density.

Marginal posteriors instead of the joint. Scientific insight is often based on a low dimensional marginalization of the posterior with nuisance parameters removed. The full joint posterior can be unnecessarily informative. Targeting marginals directly, by estimating only the marginal posterior for the parameters of interest, is simpler and sufficient for most purposes.

Consistency checks through local amortization. Practitioners are interested in testing the quality of inference methods [15–17]. One such test is to compare the empirical and nominal contained mass of estimated credible regions. *Amortized* methods learn the posterior for any data, generated by any parameter, facilitating empirical study of the nominal credible regions on fabricated data. Still, learning an amortized posterior is excessive if only a small subset of parameters are consistent with a target observation.

We propose the concept of *local amortization* to learn the posterior on said subset, combining simulator efficiency of targeted inference with the testability of amortization. Both are critical components for enabling trustworthy scientific results.

Our contribution. We propose an algorithm that simultaneously achieves all three of the above aspects: Truncated Marginal Neural Ratio Estimation (TMNRE) approximates the marginal likelihood-to-evidence ratio in a sequence of rounds. As a basis, we adopt likelihood-to-evidence estimation proposed in [8]. Our iterative scheme is loosely inspired by likelihood-based nested sampling [6, 18, 19] since we generate training data drawn from a nested sequence of truncated priors in multiple rounds. Our algorithm (a) preferentially generates simulations in relevant regions of the parameter space, (b) allows generation of all marginals of interest simultaneously and in parallel from the same training data, and (c) yields posteriors that are locally amortized in a constrained region around the posterior, enabling empirical self-consistency test of the inference results.

Related work. In Table 1, we compare the properties and features of a selection of deep-learning based simulator-based inference methods that are directly relevant for our work. Sampling from regions of highest probability density is baked into most *likelihood-based* methods [4–6, 18–22]. Amortization is generally not available with these methods because they sample from a particular posterior. *Approximate Bayesian Computation (*ABC*)* is a rejection sampling technique where proposed samples from the generative model are accepted based on a user defined distance criterion comparing generated data to the observation of interest. Two important methods include REJ-ABC [7] where the proposal distribution is simply the parameter prior and SMC-ABC [23, 24] where the proposal is iteratively refined.

Likelihood-free inference can be cast as a conditional density estimation problem targeting either the posterior directly [11–14] or the likelihood [10, 25]. This technique requires a density estimator, normally implemented as a mixture density network [26] or a normalizing flow [27, 28]. *Neural Likelihood Estimation* (NLE) performs well on benchmark tasks but must learn a density representation of the data in an unsupervised setting. Modern variants of *Neural Posterior Estimation* (NPE) [14] have become effective enough to offer an alternative marginal estimation method for practitioners. A simple implementation was discussed in [29].

*Amortized Approximate Ratio Estimators / Neural Ratio Estimation (*NRE*):* Binary classification allows estimation of the likelihood ratio between two hypotheses [9, 30–34] and was most famously applied to Generative Adversarial Networks [35]. Ref. [8] noted that naive application in the likelihood-free setting was unsatisfactory because the mathematically arbitrary choice of reference hypothesis significantly affected empirical MCMC results. Comparing likelihoods from jointly drawn $(\boldsymbol{x}, \boldsymbol{\theta}) \sim p(\boldsymbol{x}, \boldsymbol{\theta})$ and marginally drawn $(\boldsymbol{x}, \boldsymbol{\theta}) \sim p(\boldsymbol{x})p(\boldsymbol{\theta})$ samples, where $\boldsymbol{x}$ and $\boldsymbol{\theta}$ refer respectively

to simulated data and simulator parameters, addresses the issue. Ref. [14] cast NRE and NPE in a unifying framework by adapting the loss function to contrast several possible hypothetical parameters. In this paper we refer to the algorithm described in [8] as NRE or NRE_A while the likelihood ratio algorithm described in [14] is referred to as NRE_B.

Directly estimating the marginal posterior distribution directly has been mentioned [8] and explored [29, 36]. Moment networks [29] produce the (central) moments of the posterior distribution, without calculating the density explicitly, via a hierarchy of neural networks trained on a regression problem. Ref. [29] also introduced a method which learns marginal posteriors with normalizing flows.

Sequential Methods: The neural likelihood-free methods generally offer a so-called sequential formulation that targets the posterior of a particular observation $\boldsymbol{x}_o$ [8, 10, 14]. Rather than drawing samples from the prior, the simulation budget is divided between rounds and the previous round's posterior is used as the new proposal distribution for the next round. This method increases simulation efficiency, but does not allow for amortization. Importantly, sequential methods can become highly inefficient when targeting multiple marginal posteriors directly because the previous round's marginal posterior does not update beliefs about the other parameters. A full parameter vector is necessary to run the simulator, thus defeating the purpose for all nuisance (marginalized-over) parameters.

2 Method

We aim to estimate any marginal posterior of interest using an approximate marginal likelihood-to-evidence ratio. Although we normally compute every one and two dimensional marginal posterior for visualization purposes, our method is not limited to this restriction. Let us define the object of study.

Let parametric stochastic simulator $\boldsymbol{g}$ be a nonlinear function that maps a vector of real parameters $\boldsymbol{\theta} = (\theta_1, \dots, \theta_D)$ and a stochastic latent state $\boldsymbol{z}$ to an observation $\boldsymbol{x} = \boldsymbol{g}(\boldsymbol{\theta}, \boldsymbol{z})$. The likelihood function is therefore $p(\boldsymbol{x} \mid \boldsymbol{\theta}) = \int \delta(\boldsymbol{x} - \boldsymbol{g}(\boldsymbol{\theta}, \boldsymbol{z}))\, p(\boldsymbol{z} \mid \boldsymbol{\theta})\, d\boldsymbol{z}$, where $\delta(\cdot)$ denotes the Dirac delta. We consider a *factorizable prior* $p(\boldsymbol{\theta}) = p(\theta_1) \cdots p(\theta_D)$ over the parameters. The joint posterior is given via Bayes' rule as $p(\boldsymbol{\theta} \mid \boldsymbol{x}) = p(\boldsymbol{x} \mid \boldsymbol{\theta}) p(\boldsymbol{\theta}) / p(\boldsymbol{x})$, where $p(\boldsymbol{x})$ is the evidence. Our goal is to efficiently compute arbitrary marginal posteriors, $p(\boldsymbol{\vartheta} \mid \boldsymbol{x})$. Here, $\boldsymbol{\vartheta}$ are the parameters of interest, and we denote all other (nuisance) parameters by $\boldsymbol{\eta}$, such that $\boldsymbol{\theta} = (\boldsymbol{\vartheta}, \boldsymbol{\eta})$. The marginal posterior is obtained from the joint distribution $p(\boldsymbol{\vartheta}, \boldsymbol{\eta} \mid \boldsymbol{x}) \coloneqq p(\boldsymbol{\theta} \mid \boldsymbol{x})$ by integrating over all components of $\boldsymbol{\eta}$,

$$p(\boldsymbol{\vartheta} \mid \boldsymbol{x}) = \int p(\boldsymbol{\vartheta}, \boldsymbol{\eta} \mid \boldsymbol{x})\, d\boldsymbol{\eta} = \frac{\int p(\boldsymbol{x} \mid \boldsymbol{\vartheta}, \boldsymbol{\eta}) p(\boldsymbol{\eta})\, d\boldsymbol{\eta}}{p(\boldsymbol{x})} p(\boldsymbol{\vartheta}) \coloneqq \frac{p(\boldsymbol{x} \mid \boldsymbol{\vartheta})}{p(\boldsymbol{x})} p(\boldsymbol{\vartheta}). \tag{1}$$

where we used Bayes' rule, prior factorizibility, and defined the marginal likelihood $p(\boldsymbol{x} \mid \boldsymbol{\vartheta})$.

2.1 Marginal Neural Ratio Estimation (MNRE)

This paper considers the set of one and two dimensional marginal posteriors and their corresponding parameters of interest. Given parameter vector $\boldsymbol{\theta} \in \mathbb{R}^D$, define the set of all parameters associated with the one dimensional marginal posteriors by $\Theta_1 \coloneqq \{\theta_1, \dots, \theta_D\}$. We do something similar, up to symmetry, for all two dimensional marginal posteriors $\Theta_2 \coloneqq \left\{(\theta_i, \theta_j) \in \mathbb{R}^2 \;\middle|\; i = 1, \dots, D,\ j = i+1, \dots, D\right\}$. We set our marginals of interest $\{\boldsymbol{\vartheta}_k\} \coloneqq \Theta_1 \cup \Theta_2$ but in the general case, $\{\boldsymbol{\vartheta}_k\}$ can be any set of marginals that the practitioner desires. For every $\boldsymbol{\vartheta}_k$ we use NRE [8] to estimate the corresponding marginal likelihood-to-evidence ratio

$$r_k(\boldsymbol{x} \mid \boldsymbol{\vartheta}_k) \coloneqq \frac{p(\boldsymbol{x} \mid \boldsymbol{\vartheta}_k)}{p(\boldsymbol{x})} = \frac{p(\boldsymbol{x}, \boldsymbol{\vartheta}_k)}{p(\boldsymbol{x}) p(\boldsymbol{\vartheta}_k)} = \frac{p(\boldsymbol{\vartheta}_k \mid \boldsymbol{x})}{p(\boldsymbol{\vartheta}_k)}\ . \tag{2}$$

To this end, we train binary classifiers $\hat{\rho}_{k,\phi}(\boldsymbol{x}, \boldsymbol{\vartheta}_k)$ to distinguish jointly drawn parameter-simulation pairs $(\boldsymbol{x}, \boldsymbol{\vartheta}_k) \sim p(\boldsymbol{x}, \boldsymbol{\vartheta}_k)$ from marginally drawn parameter-simulation pairs $(\boldsymbol{x}, \boldsymbol{\vartheta}_k) \sim p(\boldsymbol{x}) p(\boldsymbol{\vartheta}_k)$, where ϕ represents the parameters of the classifier. A Bayes optimal classifier ρ_k would recover the density $\rho_k(\boldsymbol{x}, \boldsymbol{\vartheta}_k) = \frac{p(\boldsymbol{x}, \boldsymbol{\vartheta}_k)}{p(\boldsymbol{x}, \boldsymbol{\vartheta}_k) + p(\boldsymbol{x}) p(\boldsymbol{\vartheta}_k)}$. Then the ratios of interest can be estimated by

$$\hat{r}_k(\boldsymbol{x} \mid \boldsymbol{\vartheta}_k) \coloneqq \frac{\hat{\rho}_{k,\phi}(\boldsymbol{x}, \boldsymbol{\vartheta}_k)}{1 - \hat{\rho}_{k,\phi}(\boldsymbol{x}, \boldsymbol{\vartheta}_k)} \approx \frac{p(\boldsymbol{x}, \boldsymbol{\vartheta}_k)}{p(\boldsymbol{x}) p(\boldsymbol{\vartheta}_k)} = r_k(\boldsymbol{x} \mid \boldsymbol{\vartheta}_k)\ . \tag{3}$$

We train each ratio estimator $\hat{r}_k(\boldsymbol{x} \mid \boldsymbol{\vartheta})$ using Adam [37] to minimize the binary cross-entropy (BCE)

$$\ell_k = -\int \left[p(\boldsymbol{x} \mid \boldsymbol{\theta}) p(\boldsymbol{\theta}) \ln \hat{\rho}_{k,\phi}(\boldsymbol{x}, \boldsymbol{\vartheta}_k) + p(\boldsymbol{x}) p(\boldsymbol{\theta}) \ln\left(1 - \hat{\rho}_{k,\phi}(\boldsymbol{x}, \boldsymbol{\vartheta}_k)\right) \right] d\boldsymbol{x}\, d\boldsymbol{\theta}\ . \tag{4}$$

In practice, we concatenate $\boldsymbol{x}$ with $\boldsymbol{\vartheta}_k$ as the input to $\hat{\rho}_{k,\phi}$. Since each classifier trains independently, it is trivial to train them all in parallel using the same underlying $(\boldsymbol{x}, \boldsymbol{\theta})$ pairs.

Practically, we parameterize the classifier by $\hat{\rho}_{k,\phi}(\boldsymbol{x}, \boldsymbol{\vartheta}_k) = \sigma \circ f_{k,\phi}(\boldsymbol{x}, \boldsymbol{\vartheta}_k)$, where σ is the logistic sigmoid and $f_{k,\phi}$ is a neural network. The connection in Eq. (3) between the estimated ratio and the classifier implies that $\log \hat{r}_k(\boldsymbol{x} \mid \boldsymbol{\vartheta}_k) = f_{k,\phi}(\boldsymbol{x}, \boldsymbol{\vartheta}_k)$. We call the above technique MNRE.

When training data is limited, we found empirically (see Sec. 3.2 below) that the MNRE approach typically leads to conservative (i.e., not overconfident) likelihood-to-evidence ratio estimates, provided early stopping criteria are used to avoid over-fitting of the classifier. At its core MNRE solves a simple, supervised binary classification task rather than a complex, unsupervised density estimation problem. Classification tasks are generally easier to train [9], and can rely on battle-tested network architectures.

2.2 Truncated Marginal Neural Ratio Estimation (TMNRE)

MNRE and NRE estimate a (marginal) likelihood-to-evidence ratio agnostic to the observed data $\boldsymbol{x}$ or parameter $\boldsymbol{\theta}$, a so-called *amortized* estimate. In other words, MNRE is suitable when $\boldsymbol{x} \in \{\boldsymbol{g}(\boldsymbol{\theta}, \boldsymbol{z}) \mid \boldsymbol{\theta} \in \Omega, \forall \boldsymbol{z}\}$ where Ω is the support of the prior. We propose an extension of this algorithm that enables targeted simulation of parameters relevant to a given target observation $\boldsymbol{x}_o$, and locally amortizes posteriors such that it enables empirical tests of the inference results. *Local amortization* implies that our proposed method is suitable when $\boldsymbol{x} \in \{\boldsymbol{g}(\boldsymbol{\theta}, \boldsymbol{z}) \mid \boldsymbol{\theta} \in \Gamma, \forall \boldsymbol{z}\}$ where the parameter region $\Gamma \subset \Omega$ is a function of $\boldsymbol{x}_o$ and will be defined below.

We observe that values of $\boldsymbol{\theta}$ which could not have plausibly generated $\boldsymbol{x}_o$ evaluate to negligible posterior density, i.e. $p(\boldsymbol{\theta} \mid \boldsymbol{x}_o) \approx 0$, which suggests that the corresponding parameters $\boldsymbol{\theta}$ do not significantly contribute to the marginalization in Eq. (1). We denote a prior that is suitably constrained to parameters with non-negligible posterior density $p(\boldsymbol{\theta} \mid \boldsymbol{x}_o)$ by

$$p_\Gamma(\boldsymbol{\theta}) \coloneqq V^{-1} \mathbb{1}_\Gamma(\boldsymbol{\theta}) p(\boldsymbol{\theta}) \,, \tag{5}$$

where $\mathbb{1}_\Gamma(\boldsymbol{\theta})$ is an indicator function that is unity on $\Gamma \subset \Omega$ and zero otherwise, and V^{-1} is a normalizing constant (which can be interpreted as the fractional volume of the truncated prior). The subscript $\square_\Gamma$ denotes quantities $\square$ based on a prior truncated by indicator function $\mathbb{1}_\Gamma$.

We define a rectangular indicator function $\mathbb{1}_{\Gamma^{\text{rec}}}$ by discarding parameters that lie in the far tails of the one dimensional marginal posteriors of our target observation $\boldsymbol{x}_o$, using a thresholding $\epsilon \ll 1$, via

$$\Gamma^{\text{rec}} = \left\{ \boldsymbol{\theta} \in \Omega \;\middle|\; \forall d = 1, \dots, D : \frac{p(\theta_d \mid \boldsymbol{x}_o)}{\max_{\theta_d} p(\theta_d \mid \boldsymbol{x}_o)} > \epsilon \right\} \,. \tag{6}$$

For Gaussian joint posteriors, this scheme leads to one dimensional marginal posteriors $p_\Gamma(\theta_d \mid \boldsymbol{x}_o)$ that are truncated at their approximately $\pm\sqrt{-2 \ln \epsilon}\sigma$ tail. In general, truncation will lead to an approximation error that can be estimated as $p_{\Gamma^{\text{rec}}}(\boldsymbol{\theta} \mid \boldsymbol{x}_o) = p(\boldsymbol{\theta} \mid \boldsymbol{x}_o) + \mathcal{O}(\epsilon) \max_{\boldsymbol{\theta}} p(\boldsymbol{\theta} \mid \boldsymbol{x}_o)$, see Appendix C. Throughout this paper, we use $\epsilon = 10^{-6}$, which corresponds to $\pm 5.26\sigma$ for a Gaussian posterior. Those truncations do not affect the location of high-probability credible contours and have hence no practical effect on parameter inference tasks. We provide more exemplary error estimates for a range of cases in Appendix C.

Our algorithm defines a series of nested indicator functions $\mathbb{1}_{\Gamma^{(m)}}$ whose regions have the property

$$\Omega \coloneqq \Gamma^{(1)} \supset \Gamma^{(2)} \supset \cdots \supset \Gamma^{(M)} \supset \Gamma^{\text{rec}}. \tag{7}$$

They iteratively approximate the indicator function $\mathbb{1}_{\Gamma^{\text{rec}}}$ in multiple rounds $m = 1, \dots, M$. This sequence is generated with the following steps:

- We initialize $\Gamma^{(1)} = \Omega$, meaning that we start with the unconstrained prior.
- Each round $1 \leq m \leq M$, we train D, one dimensional ratio estimators $\hat{r}_{d,\Gamma^{(m)}}(\boldsymbol{x} \mid \theta_d)$ using data from within the constrained region, $\boldsymbol{\theta} \in \Gamma^{(m)}$. The estimated marginal posterior is $\hat{p}_{\Gamma^{(m)}}(\theta_d \mid \boldsymbol{x}) = \hat{r}_{d,\Gamma^{(m)}}(\boldsymbol{x} \mid \theta_d) p_{\Gamma^{(m)}}(\theta_d)$. To this end, do MNRE, setting $\boldsymbol{\vartheta}_k = \theta_k,\ d \in \{1, 2, \dots, D\}$ using the constrained prior $p_{\Gamma^{(m)}}(\boldsymbol{\theta})$ with $N^{(m)}$ training samples per round.
- For each round $m < M$, we estimate the indicator function for the next round using the approximated posteriors, via

$$\Gamma^{(m+1)} = \left\{ \boldsymbol{\theta} \in \Gamma^{(m)} \;\middle|\; \forall d : \frac{\hat{p}_{\Gamma^{(m)}}(\theta_d \mid \boldsymbol{x}_o)}{\max_{\theta_d} \hat{p}_{\Gamma^{(m)}}(\theta_d \mid \boldsymbol{x}_o)} > \epsilon \right\} \,. \tag{8}$$

Algorithm 1 Truncated Marginal Neural Ratio Estimation (TMNRE)

Inputs: Simulator $p(\boldsymbol{x} \mid \boldsymbol{\theta})$, factorizable prior $p(\boldsymbol{\theta})$, real observation $\boldsymbol{x}_0$, max rounds M, training data per round $N^{(m)}$, threshold ϵ, dimension of parameters D, mass ratio β, classifiers $\boldsymbol{\rho}_1(\boldsymbol{x}, \boldsymbol{\theta}) = \{\sigma \circ f_{\phi,d}(\boldsymbol{x}, \theta_d)\}_{d=1}^{D}$ and $\boldsymbol{\rho}_2(\boldsymbol{x}, \boldsymbol{\theta}) = \{\sigma \circ f_{\phi,d}(\boldsymbol{x}, \boldsymbol{\vartheta}_d)\}_{d=(1,1)}^{(D,D)}$.

Outputs: Parameterized classifiers $\boldsymbol{\rho}_1(\boldsymbol{x}, \boldsymbol{\theta})$ and $\boldsymbol{\rho}_2(\boldsymbol{x}, \boldsymbol{\theta})$, constrained region Γ^{rec}.

procedure MNRE($\mathcal{D}$, $\boldsymbol{\theta}'$, $\boldsymbol{\rho}_\phi$)
  while $\boldsymbol{\rho}_\phi$ not converged **do**
    $\phi \leftarrow \text{OPTIMIZER}\left(\phi, \nabla_\phi \sum_k \left[\text{BCE}(\hat{\rho}_{\phi,k}(\boldsymbol{x}, \boldsymbol{\vartheta}_k), 1) + \text{BCE}(\hat{\rho}_{\phi,k}(\boldsymbol{x}, \boldsymbol{\vartheta}'_k), 0)\right]\right)$
  return $\mathbf{f}_\phi$

Initialize: $\mathcal{D}^{(0)} \leftarrow \{\}$, $\Gamma^{(0)} \leftarrow \text{supp}(p(\boldsymbol{\theta}))$, $\alpha^{(0)} \leftarrow 0$, $m \leftarrow 1$.

procedure TMNRE
  while $\alpha^{(m-1)} \leq \beta$ and $m \leq M$ **do**
    $\mathcal{D}_\Gamma^{(m-1)} \leftarrow \left\{(\boldsymbol{x}^{(n)}, \boldsymbol{\theta}^{(n)}) \in \mathcal{D}^{(m-1)} \;\middle|\; \boldsymbol{\theta}^{(n)} \in \Gamma^{(m-1)}\right\}$ ▷ *Retain data in region*
    $N_{\text{simulate}}^{(m)} \leftarrow N^{(m)} - |\mathcal{D}_\Gamma^{(m-1)}|$ ▷ *Calculate num. necessary simulations*
    $\boldsymbol{\theta} \leftarrow \{\boldsymbol{\theta}^{(n)} \sim \mathbb{1}_{\Gamma^{(m-1)}}(\boldsymbol{\theta}) p(\boldsymbol{\theta})\}_{n=1}^{N_{\text{simulate}}^{(m)}}$ ▷ *Sample for jointly distributed pairs*
    $\boldsymbol{x} \leftarrow \{\boldsymbol{x}^{(n)} \sim p(\boldsymbol{x} \mid \boldsymbol{\theta}^{(n)})\}_{n=1}^{N_{\text{simulate}}^{(m)}}$ ▷ *Simulate jointly distributed pairs*
    $\boldsymbol{\theta}' \leftarrow \{\boldsymbol{\theta}^{(n)} \sim \mathbb{1}_{\Gamma^{(m-1)}}(\boldsymbol{\theta}) p(\boldsymbol{\theta})\}_{n=1}^{N^{(m)}}$ ▷ *Sample for marginally distributed pairs*
    $\mathcal{D}^{(m)} \leftarrow \mathcal{D}_\Gamma^{(m-1)} \cup \{(\boldsymbol{x}^{(n)}, \boldsymbol{\theta}^{(n)})\}_{n=1}^{N_{\text{simulate}}^{(m)}}$ ▷ *Aggregate training data*
    $\boldsymbol{\rho}_1 \leftarrow \text{MNRE}(\mathcal{D}^{(m)}, \boldsymbol{\theta}', \boldsymbol{\rho}_1)$
    $\Gamma^{(m)} \leftarrow \left\{\boldsymbol{\theta} \in \Gamma^{(m-1)} \;\middle|\; \forall d : \frac{\hat{p}_{d,\Gamma^{(m)}}(\theta_d | \boldsymbol{x}_o)}{\max_{\theta_d} \hat{p}_{d,\Gamma^{(m)}}(\theta_d | \boldsymbol{x}_o)} > \epsilon\right\}$ ▷ *Find constrained region*
    $\alpha^{(m)} \leftarrow \int \mathbb{1}_{\Gamma^{(m)}}(\boldsymbol{\theta}) p(\boldsymbol{\theta}) d\boldsymbol{\theta} / \int \mathbb{1}_{\Gamma^{(m-1)}}(\boldsymbol{\theta}) p(\boldsymbol{\theta}) d\boldsymbol{\theta}$ ▷ *Update prior mass ratio*
    $m \leftarrow m + 1$ ▷ *Increment counter*
  $\boldsymbol{\rho}_2 \leftarrow \text{MNRE}(\mathcal{D}^{(m)}, \boldsymbol{\theta}', \boldsymbol{\rho}_2)$
  return $\boldsymbol{\rho}_1$, $\boldsymbol{\rho}_2$, $\Gamma^{(m)}$

- The last round is determined either when $m = M$ or when a stopping criterion is reached. The stopping criterion is defined by the ratio of consecutive truncated prior masses. It is satisfied when the sequence of truncated priors have the property $\int \mathbb{1}_{\Gamma^{(m)}}(\boldsymbol{\theta}) p(\boldsymbol{\theta}) d\boldsymbol{\theta} / \int \mathbb{1}_{\Gamma^{(m-1)}}(\boldsymbol{\theta}) p(\boldsymbol{\theta}) d\boldsymbol{\theta} > \beta$. We often set $\beta = 0.8$.
- Using the data from this final constrained region, we train all one and higher-dimensional marginal posteriors of interest.

We briefly address failure modes. First, this algorithm relies on the assumption that posterior estimates $\hat{p}_{\Gamma^{(m)}}(\theta_d \mid \boldsymbol{x}_o)$ from MNRE provide a good approximation of $p(\theta_d \mid \boldsymbol{x}_o)$. An over-confident estimate would remove parameter ranges that are part of Γ^{rec}. In practice, we have not observed this effect. We give credit to early stopping and a conservative choice of ϵ, and provide further illustration and support in Sec. 3 below. Second, since the truncated posterior only agrees with the ground truth up to corrections of order ϵ, the iterative scheme will not converge to Eq. (6); rather to a similar expression where the right-hand side of the inequality in Eq. (6) receives additional $\mathcal{O}(\epsilon)$ corrections. Although these corrections mildly affect the truncations, they are of little practical relevance since we choose an ϵ which is very small. Both failure modes are diagnosed by checking whether high probability regions of the estimated posteriors intersect with the boundaries of the indicator function.

Like sequential methods [10, 14] the number of rounds M, the training data per round $N^{(m)}$, and any stopping criteria β are hyperparameters. For further discussion and default values see Appendix A, for bound derivations and limitations see Appendix C and D. We present TMNRE in Algorithm 1.

Properties of our algorithm. We discuss the properties of our algorithm in support of Table 1. First, our algorithm performs *targeted inference* by successively focusing on regions of the parameter space that are compatible with an observation $\boldsymbol{x}_o$. Second, since training data is always drawn from the prior, it is possible to efficiently *train arbitrary marginal posteriors* with the same training data generated for round M. Third, the algorithm trains *locally amortized posteriors* that are valid for

parameters $\boldsymbol{\theta} \in \Gamma^{(m)}$, facilitating empirical consistency checks of the estimated posteriors within this region. All these aspects will be demonstrated in the experiments in the following section.

3 Experiments

First, we perform experiments to compare TMNRE to other algorithms on standard benchmarks from the simulator-based inference literature. Next, we highlight useful aspects of our algorithm regarding targeted inference, marginalization and local amortization with two additional experiments. Further experiments, including application on a cosmology simulator, can be found in Appendix E.

3.1 Performance on standard tasks

We compare the performance of our algorithm with other traditional and neural simulation-based inference methods on a selection of problems from the SBI benchmark [38]. Each *task* is defined by a simulator, ten observations, a simulation budget, and 10,000 samples drawn from corresponding reference and approximate posterior distributions. The reference samples enable quantification of algorithmic accuracy on a range of performance metrics. We evaluate performance on each of the following tasks: Gaussian Linear Uniform, SLCP, SLCP Distractors, Gaussian Mixture, and Two Moons. Each has a uniform prior. Details in Appendix A.

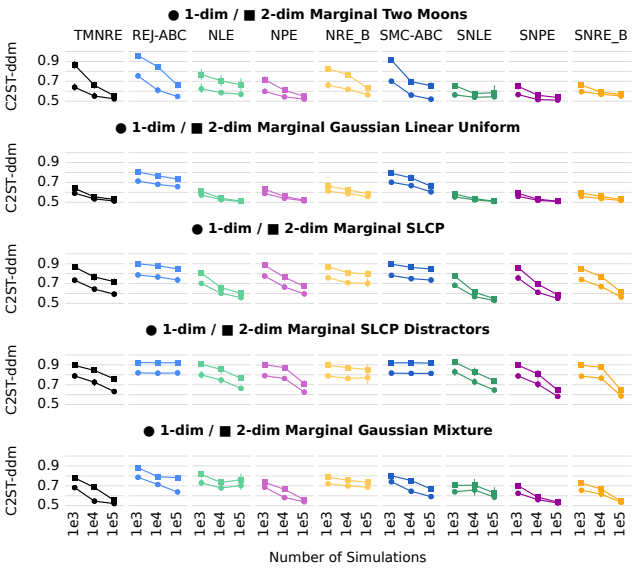

Figure 1: **Performance on marginalized posterior benchmark tasks.** Classification accuracy (C2ST-ddm) of our method, TMNRE, and REJ-ABC, NLE, NPE, NRE_B, SMC-ABC, SNLE, SNPE, and SNRE_B for 10 observations each, means and 95% confidence intervals. One and two dimensional scores are plotted. Lower scores imply better posteriors. Our simulation budget is approximate but within $\sim 5\%$ of reported value. The plot and tasks are derivative of [38].

Since our method estimates every one and two dimensional marginal posterior, we compare samples from our approximate marginal posteriors with samples from the reference joint posterior, marginalized over nuisance parameters. We quantify the results using the Classifier 2-Sample Test [39, 40]. We train a C2ST classifier for each of the $\binom{D}{1} + \binom{D}{2}$ possible one and two dimensional marginals, and report the mean values, and 95% confidence intervals, in Figure 1. We call this averaged performance metric *C2ST-ddm*, see Appendix B for more detail. The results are presented as grouped by dimensionality since learning difficulty increases with dimension and we expect this to be reflected in the C2ST-ddm scores.

For comparison, we computed the C2ST-ddm on the other benchmark methods' posterior samples. Unlike our method, which was trained on the marginals directly, the benchmark methods were trained to estimate the joint posterior. We note that since TMNRE trains a neural network for every marginal (efficiently, in parallel), our method has many times more parameters than any neural likelihood-free inference method that directly targets the joint. However, parameter count is not usually a scarce resource in this setting. Training hyperparameters can be found in Appendix A.

As shown in Figure 1, our method outperformed both REJ-ABC and SMC-ABC on all tasks. The maximum number of rounds before meeting the stopping criteria was four for Two Moons, Gaussian Linear Uniform, and Gaussian Mixture. TMNRE was competitive with sequential methods at high simulation budget on these tasks, while it performed only slightly better than non-sequential methods on the SLCP and SLCP Distractors. TMNRE stopped after only two and one round(s) on SLCP

and SLCP Distractors. Doing marginal inference directly offers increased efficiency compared to non-sequential methods across tasks. On the tasks with narrow posteriors, it offered comparable accuracy with sequential methods given large simulation budget, The benefit was diminished on tasks with wide posteriors like SLCP and SLCP Distractors–a limitation of the method. In general, TMNRE provides sufficient accuracy and local amortization. Neither sequential nor non-sequential methods offer both.

3.2 Efficient targeted inference: a 3-dim torus model

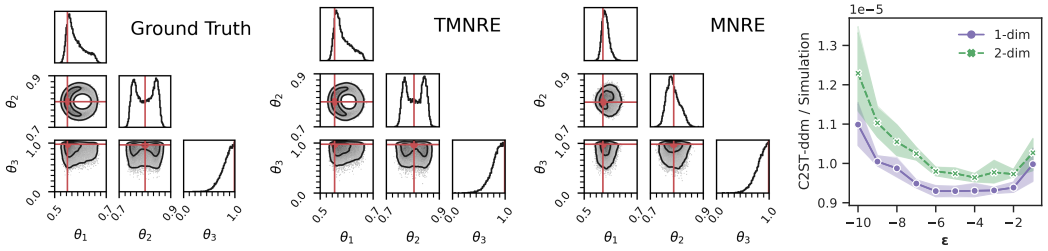

Figure 2: *First through Third Panel:* View of torus marginal posteriors as estimated by rejection sampling, TMNRE, and MNRE. In some dimensions, the posterior extends the full unit cube prior width, while in others it is very narrow. TMNRE easily finds the asymmetric details after constraining to the relevant region while MNRE does not. *Fourth Panel:* The results of a hyperparameter scan of ϵ on the torus task. The C2ST-ddm per simulation is reported versus ϵ. The mean and 95% confidence intervals are shown over five repetitions of the experiment. Lower values indicate better performance.

We define a task which highlights the effectiveness of truncating the prior, namely a simulator with a very small torus shaped posterior. We present an ablation study of the truncation method along with a hyperparameter scan of ϵ. The task's details are enumerated in Appendix A.

We ran Algorithm 1 which satisfied the stopping criterion after four rounds. We performed marginal likelihood-to-evidence ratio estimation on all one and two dimensional marginals for each step in the sequence of constrained regions, using the number of samples available that round. We also trained an estimator which used the same simulation budget but the samples were drawn from the unconstrained prior. We analyzed the prior volume, C2ST-ddm, and the sum of one dimensional KL divergences at each round for both methods. The posteriors are shown in Figure 2 and the performance metrics for the ablation study, are shown in Figure 3.

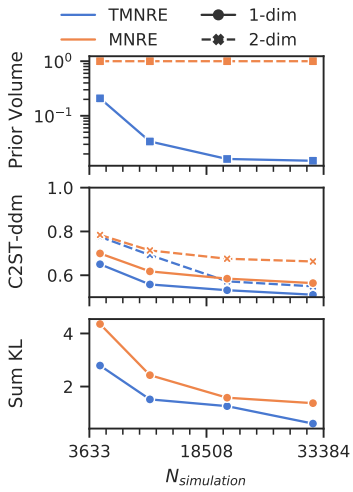

Figure 3: Performance metrics on MNRE and TMNRE versus simulation budget. Budgets determined by truncation algorithm. *T:* Prior volume. *M:* According to C2ST-ddm, TMNRE produces more accurate posteriors. *L:* KL divergence summed over 1-dim marginals; same result.

We found TMNRE very accurately approximated all marginals at the maximum simulation budget. MNRE placed mass in the correct region but missed the shape of the posterior entirely. TMNRE improved simulation efficiency compared with MNRE as indicated by the slope of the C2ST-ddm. The max-normalized posterior estimates at every round are plotted in Figure 4. We note that given the limited training data in early rounds, our method predicts wider posteriors than the ground truth. These are called conservative posterior estimates and they are the preferred failure mode for practitioners.

To determine the effects the hyperparameter ϵ, we performed a grid search between 10^{-10} to 10^{-1} using TMNRE on the same simulator. We reported the performance in terms of the C2ST-ddm per simulation in Figure 2 and repeated the experiment five times. We observe that the optimal value of ϵ was 10^{-6} since it was the most conservative value of ϵ that optimized the metric.

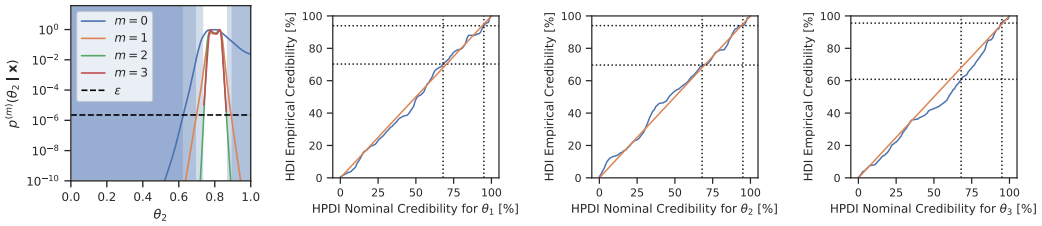

Figure 4: *First panel:* The ratio estimator for θ_2 in the 3-dim torus example, for several consecutive rounds. The estimator is conservative with limited data because it converges from above against the final results (red line). *Second to Fourth Panels:* Empirical versus nominal credibility for the highest posterior density intervals (HPDI) for each θ_d in the 3-dim torus.

3.3 Empirical tests of inference results through local amortization

Our algorithm locally amortizes the posterior for parameters drawn from the constrained prior $p_\Gamma(\boldsymbol{\theta})$. This opens the door for various experimental diagnostics to test the reliability of our trained inference networks with simulated data (which is also possible for NRE [41], but not for sequential methods that are exclusively targeting on one specific observation rather than a range of observations). We demonstrate this by comparing the empirical credibility to the nominal credibility for the highest posterior density intervals.

For the 3-dim torus example, we draw 10000 samples $(\boldsymbol{x}, \theta_d) \sim p(\boldsymbol{x} \mid \boldsymbol{\theta}) p_\Gamma(\boldsymbol{\theta})$ from the constrained generative model. For all samples, we generate marginal posteriors, $\hat{p}(\theta_d \mid \boldsymbol{x})$. For those marginal posteriors, we then derive the frequency with which $t\%$ highest density intervals contain the true value θ_d. The result is shown in Fig. 4. It provides an immediate check of the reliability of our trained inference networks *without knowing the ground truth*, and provides a safeguard against overconfident statements, which is critical for using the results of inference networks in a scientific context.

3.4 Efficient marginal posteriors: a 10-dim egg-box model

We define a posterior that, when plotted in two dimensions, looks like a top-down view of an 2×2 egg-box. Let $\boldsymbol{\theta}, \boldsymbol{g}(\boldsymbol{\theta}) \in \mathbb{R}^D$ and θ_k denote the kth element of $\boldsymbol{\theta}$, then the simulator for this problem is defined $g_k(\boldsymbol{\theta}) = \sin(\theta_k \cdot \pi)$. To fix the posterior shape, we set $\theta_{k,o} = \frac{1}{4}$, $k = 1, 2, \ldots, D$ and $\boldsymbol{x}_0 = \boldsymbol{g}(\boldsymbol{\theta}_o)$. The likelihood is determined by an additive noise model $p(\boldsymbol{x} \mid \boldsymbol{\theta}) = \mathcal{N}(\boldsymbol{g}(\boldsymbol{\theta}), \sigma^2 \boldsymbol{I})$ with $\sigma = 0.1$. The total number of modes in our 10-dimensional model is $2^{10} = 1024$. Realistic models do not typically feature such a regular mode structure, but this pattern enables an analytic estimate of ground truth posteriors for comparison with the various algorithms.

Given 10,000 training samples drawn from the prior and a $D = 10$ dimensional parameter space, we trained MNRE to estimate all one and two dimensional marginals, the SBI [42] implementation of NRE and SNRE on the joint, and finally a marginalized version of SNRE (SMNRE). In SMNRE, we divided the samples across 10 rounds and each round proposed samples according to the previous round's posterior distribution for the predicted marginals, but the initial prior for the nuisance parameters. Since, in a general setting, SMNRE cannot use samples from another marginal estimator, we divided the 10,000 training samples evenly among the 55, one and two dimensional marginal estimators, each estimator receiving 181 training samples. 25,000 samples from each reported posterior are visible in Figure 5. Our method was the only one which recovered the structure of the ground truth marginal posteriors, providing empirical evidence that estimating marginals directly can provide high accuracy at low simulation budgets for complex high-dimensional posteriors.

4 Discussion and conclusions

We presented Truncated Marginal Neural Ratio Estimation (TMNRE), a simulation-based inference algorithm based on NRE. The core idea of our algorithm is to focus on most probable parameter regions by truncating marginal posteriors in their very low-probability tails. For Gaussian posteriors this is typically beyond 5σ and does not significantly affect the higher density contours. In addition to performing on par or better than existing algorithms on standard benchmarks, TMNRE is better

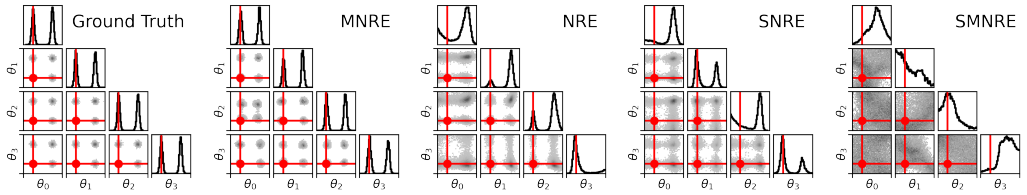

Figure 5: Posteriors from the 10-dim eggbox benchmark (only 4 parameters are shown for clarity). All methods received 10k training samples and produced 25k posterior samples. NRE and SNRE were trained jointly, while MNRE and SMNRE were trained marginally. SMNRE cannot share training samples between marginals so each estimator received an equal share of the total simulation budget, 181 samples. Our method is the only one which recovered the structure of the ground truth.

suited to the practitioner's needs than other algorithms because it offers simulation efficient marginal posterior estimation and the capacity to perform efficient consistency checks through local amortization. These features are particularly desirable to scientists whose simulators are expensive and rife with nuisance parameters.

TMNRE uses a sequence of training and sampling rounds to automatically produce parameters with high posterior density, i.e. relevant to a particular observation $\boldsymbol{x}_o$. The output of this sequence is a hyperrectangular approximation to a highest posterior density region, implicitly defined by hyperparameter ϵ. That means simulations from within this constrained region are likely informative while simulations from outside the region are likely uninformative. Using data drawn from this constrained region, TMNRE estimates any marginal posterior of interest directly using a marginal likelihood-to-evidence ratio; a simpler and more practical technique than estimating the entire joint posterior. Finally, by construction, our targeted inference method can accurately estimate posteriors of simulations from within the constrained parameter region. This freedom facilitates fast empirical studies of the nominal credible regions, which are of critical importance in real-life applications when there is no ground truth posterior to compare to.

On the SBI benchmark [38], we found that TMNRE is on par with the most effective SBI algorithms, such as SNRE [8], as measured by the C2ST performance metric, Fig. 1. We highlighted the benefits of TMNRE using two showcase tasks: a torus-shaped posterior and an eggbox-shaped posterior. The torus featured a very narrow posterior that TMNRE found and accurately learned while simple MNRE failed to do so, Fig. 3. We demonstrated validity of our iterative procedure, and the ability to perform important validation tests by testing the nominal credible intervals empirically, Fig. 4. The eggbox's joint posterior featured 1024 modes. MNRE efficiently estimated the marginal posteriors whereas other algorithms which estimate the joint posterior on the same task generally showed low performance, Fig. 5.

The presented algorithm is aimed at marginal posterior inference, which is a typical goal for scientific applications, but does not allow, e.g., to evaluate the posterior predictive distribution which requires the joint posterior. Furthermore, our algorithm particularly shines for high-dimensional problems with complex and/or narrow posteriors, whereas we expect that simpler problems could benefit from some of the other available SBI method. We address further limitations of our method in Appendix D.

We note that the hyperrectangular indicator function, defined in Eq. (8), is not optimal if some of the parameters are strongly correlated. However, it can be straightforwardly extended to more complex shapes. The challenge is to efficiently define the boundaries of the indicator function and sample from within it, a problem tackled by effective nested sampling algorithms [43].

This work is primarily foundational and the societal impacts, other than the cost of training machine learning models, would therefore be drawn from a hypothetical application. As this is an inference method, it would be possible to apply it to biased simulators which could reinforce unethical patterns. This could go unnoticed if the simulator was too complex to assess ethically. We urge caution when applying the method to problems which could reasonably affect living things. On the other hand, this work was inspired by necessity from astrophysical problems and is already being applied to simulators which produce general public engagement in science such as understanding gravitational waves and the history of the universe, see Appendix E. In general, the societal impacts are closely tied to the implications of the simulators themselves.

Acknowledgments and Disclosure of Funding

This work uses `numpy` [44], `scipy` [45], `seaborn` [46], `matplotlib` [47], `altair` [48, 49], `pandas` [50, 51] `pytorch` [52], and `jupyter` [53]. Benjamin Kurt Miller is funded by the University of Amsterdam Faculty of Science (FNWI), Informatics Institute (IvI), and the Institute of Physics (IoP).

We want to thank the DAS-5 computing cluster for access to their TitanX GPUs. We received funding from the European Research Council (ERC) under the European Union's Horizon 2020 research and innovation programme (Grant agreement No. 864035 – UnDark).

References

[1] Nilanjan Banik, Gianfranco Bertone, Jo Bovy, and Nassim Bozorgnia. Probing the nature of dark matter particles with stellar streams. *Journal of Cosmology and Astroparticle Physics*, 2018(07):061–061, Jul 2018.

[2] Justin Alsing, Tom Charnock, Stephen Feeney, and Benjamin Wandelt. Fast likelihood-free cosmology with neural density estimators and active learning. *Monthly Notices of the Royal Astronomical Society*, 488(3):4440–4458, 2019.

[3] Johann Brehmer, Kyle Cranmer, Gilles Louppe, and Juan Pavez. Constraining effective field theories with machine learning. *Physical review letters*, 121(11):111801, 2018.

[4] Nicholas Metropolis, Arianna W Rosenbluth, Marshall N Rosenbluth, Augusta H Teller, and Edward Teller. Equation of state calculations by fast computing machines. *J. Chem. Phys.*, 21(6):1087–1092, June 1953.

[5] W K Hastings. Monte carlo sampling methods using markov chains and their applications. *Biometrika*, 57(1):97–109, April 1970.

[6] John Skilling. Nested sampling for general bayesian computation. *Bayesian Anal.*, 1(4):833–859, December 2006.

[7] Scott A Sisson, Yanan Fan, and Mark Beaumont. *Handbook of approximate Bayesian computation*. CRC Press, 2018.

[8] Joeri Hermans, Volodimir Begy, and Gilles Louppe. Likelihood-free mcmc with amortized approximate ratio estimators. In *International Conference on Machine Learning*, pages 4239–4248. PMLR, 2020.

[9] Kyle Cranmer, Johann Brehmer, and Gilles Louppe. The frontier of simulation-based inference. *Proc. Natl. Acad. Sci. U. S. A.*, May 2020.

[10] George Papamakarios, David Sterratt, and Iain Murray. Sequential neural likelihood: Fast likelihood-free inference with autoregressive flows. In *The 22nd International Conference on Artificial Intelligence and Statistics*, pages 837–848. PMLR, 2019.

[11] David Greenberg, Marcel Nonnenmacher, and Jakob Macke. Automatic posterior transformation for likelihood-free inference. In *International Conference on Machine Learning*, pages 2404–2414. PMLR, 2019.

[12] George Papamakarios and Iain Murray. Fast ϵ-free inference of simulation models with bayesian conditional density estimation. In D. Lee, M. Sugiyama, U. Luxburg, I. Guyon, and R. Garnett, editors, *Advances in Neural Information Processing Systems*, volume 29. Curran Associates, Inc., 2016.

[13] Jan-Matthis Lueckmann, Pedro J Gonçalves, Giacomo Bassetto, Kaan Öcal, Marcel Nonnenmacher, and Jakob H Macke. Flexible statistical inference for mechanistic models of neural dynamics. In *Proceedings of the 31st International Conference on Neural Information Processing Systems*, pages 1289–1299, 2017.

[14] Conor Durkan, Iain Murray, and George Papamakarios. On contrastive learning for likelihood-free inference. In *International Conference on Machine Learning*, pages 2771–2781. PMLR, 2020.

[15] Gary J Feldman and Robert D Cousins. Unified approach to the classical statistical analysis of small signals. *Physical Review D*, 57(7):3873, 1998.

[16] Alex Geringer-Sameth, Savvas M Koushiappas, and Matthew G Walker. Comprehensive search for dark matter annihilation in dwarf galaxies. *Physical Review D*, 91(8):083535, 2015.

[17] Sara Algeri, Jan Conrad, and David A van Dyk. A method for comparing non-nested models with application to astrophysical searches for new physics. *Monthly Notices of the Royal Astronomical Society: Letters*, 458(1):L84–L88, 2016.

[18] F Feroz, M P Hobson, and M Bridges. MultiNest: an efficient and robust bayesian inference tool for cosmology and particle physics. *Mon. Not. Roy. Astron. Soc. 398: 1601-1614,2009*, September 2008.

[19] W J Handley, M P Hobson, and A N Lasenby. polychord : next-generation nested sampling. *Mon. Not. R. Astron. Soc.*, 453(4):4384–4398, September 2015.

[20] Ulf Grenander and Michael I Miller. Representations of knowledge in complex systems. *Journal of the Royal Statistical Society: Series B (Methodological)*, 56(4):549–581, 1994.

[21] Gareth O Roberts, Richard L Tweedie, et al. Exponential convergence of langevin distributions and their discrete approximations. *Bernoulli*, 2(4):341–363, 1996.

[22] Gareth O Roberts and Jeffrey S Rosenthal. Optimal scaling of discrete approximations to langevin diffusions. *Journal of the Royal Statistical Society: Series B (Statistical Methodology)*, 60(1):255–268, 1998.

[23] Tina Toni, David Welch, Natalja Strelkowa, Andreas Ipsen, and Michael P H Stumpf. Approximate bayesian computation scheme for parameter inference and model selection in dynamical systems. *J. R. Soc. Interface*, 6(31):187–202, February 2009.

[24] Mark A Beaumont, Jean-Marie Cornuet, Jean-Michel Marin, and Christian P Robert. Adaptive approximate bayesian computation. *Biometrika*, 96(4):983–990, 2009.

[25] Jan-Matthis Lueckmann, Giacomo Bassetto, Theofanis Karaletsos, and Jakob H Macke. Likelihood-free inference with emulator networks. In *Symposium on Advances in Approximate Bayesian Inference*, pages 32–53. PMLR, 2019.

[26] Christopher M Bishop. Pattern recognition and machine learning (information science and statistics), 2006.

[27] George Papamakarios, Theo Pavlakou, and Iain Murray. Masked autoregressive flow for density estimation. In *Proceedings of the 31st International Conference on Neural Information Processing Systems*, pages 2335–2344, 2017.

[28] George Papamakarios, Eric Nalisnick, Danilo Jimenez Rezende, Shakir Mohamed, and Balaji Lakshminarayanan. Normalizing flows for probabilistic modeling and inference. *arXiv preprint arXiv:1912.02762*, 2019.

[29] Niall Jeffrey and Benjamin D Wandelt. Solving high-dimensional parameter inference: marginal posterior densities & moment networks. *arXiv preprint arXiv:2011.05991*, 2020.

[30] Kyle Cranmer, Juan Pavez, and Gilles Louppe. Approximating likelihood ratios with calibrated discriminative classifiers. *arXiv preprint arXiv:1506.02169*, 2015.

[31] Shakir Mohamed and Balaji Lakshminarayanan. Learning in implicit generative models. *arXiv preprint arXiv:1610.03483*, 2016.

[32] Michael U Gutmann, Jukka Corander, et al. Bayesian optimization for likelihood-free inference of simulator-based statistical models. *Journal of Machine Learning Research*, 2016.

[33] Owen Thomas, Ritabrata Dutta, Jukka Corander, Samuel Kaski, Michael U Gutmann, et al. Likelihood-free inference by ratio estimation. *Bayesian Analysis*, 2016.

[34] Dustin Tran, Rajesh Ranganath, and David M Blei. Hierarchical implicit models and likelihood-free variational inference. *arXiv preprint arXiv:1702.08896*, 2017.

[35] Ian Goodfellow, Jean Pouget-Abadie, Mehdi Mirza, Bing Xu, David Warde-Farley, Sherjil Ozair, Aaron Courville, and Yoshua Bengio. Generative adversarial networks. *Communications of the ACM*, 63(11):139–144, 2020.

[36] Benjamin Kurt Miller, Alex Cole, Gilles Louppe, and Christoph Weniger. Simulation-efficient marginal posterior estimation with swyft: stop wasting your precious time. *arXiv preprint arXiv:2011.13951*, 2020.

[37] Diederik P Kingma and Jimmy Lei Ba. Adam: A method for stochastic gradient descent. In *ICLR: International Conference on Learning Representations*, pages 1–15, 2015.

[38] Jan-Matthis Lueckmann, Jan Boelts, David Greenberg, Pedro Goncalves, and Jakob Macke. Benchmarking simulation-based inference. In Arindam Banerjee and Kenji Fukumizu, editors, *Proceedings of The 24th International Conference on Artificial Intelligence and Statistics*, volume 130 of *Proceedings of Machine Learning Research*, pages 343–351. PMLR, 13–15 Apr 2021.

[39] Jerome H Friedman. On multivariate goodness–of–fit and two–sample testing. *STATISTICAL PROBLEMS IN PARTICLE PHYSICS, ASTROPHYSICS AND COSMOLOGY*, page 311, 2003.

[40] David Lopez-Paz and Maxime Oquab. Revisiting classifier two-sample tests. In *International Conference on Learning Representations*, 2017.

[41] Joeri Hermans, Nilanjan Banik, Christoph Weniger, Gianfranco Bertone, and Gilles Louppe. Towards constraining warm dark matter with stellar streams through neural simulation-based inference. *arXiv preprint arXiv:2011.14923*, 2020.

[42] Alvaro Tejero-Cantero, Jan Boelts, Michael Deistler, Jan-Matthis Lueckmann, Conor Durkan, Pedro J. Gonçalves, David S. Greenberg, and Jakob H. Macke. sbi: A toolkit for simulation-based inference. *Journal of Open Source Software*, 5(52):2505, 2020.

[43] Edward Higson, Will Handley, Michael Hobson, and Anthony Lasenby. Dynamic nested sampling: an improved algorithm for parameter estimation and evidence calculation. *Statistics and Computing*, 29(5):891–913, 2019.

[44] Charles R. Harris, K. Jarrod Millman, St'efan J. van der Walt, Ralf Gommers, Pauli Virtanen, David Cournapeau, Eric Wieser, Julian Taylor, Sebastian Berg, Nathaniel J. Smith, Robert Kern, Matti Picus, Stephan Hoyer, Marten H. van Kerkwijk, Matthew Brett, Allan Haldane, Jaime Fern'andez del R'ıo, Mark Wiebe, Pearu Peterson, Pierre G'erard-Marchant, Kevin Sheppard, Tyler Reddy, Warren Weckesser, Hameer Abbasi, Christoph Gohlke, and Travis E. Oliphant. Array programming with NumPy. *Nature*, 585(7825):357–362, September 2020.

[45] Pauli Virtanen, Ralf Gommers, Travis E. Oliphant, Matt Haberland, Tyler Reddy, David Cournapeau, Evgeni Burovski, Pearu Peterson, Warren Weckesser, Jonathan Bright, Stéfan J. van der Walt, Matthew Brett, Joshua Wilson, K. Jarrod Millman, Nikolay Mayorov, Andrew R. J. Nelson, Eric Jones, Robert Kern, Eric Larson, C J Carey, İlhan Polat, Yu Feng, Eric W. Moore, Jake VanderPlas, Denis Laxalde, Josef Perktold, Robert Cimrman, Ian Henriksen, E. A. Quintero, Charles R. Harris, Anne M. Archibald, Antônio H. Ribeiro, Fabian Pedregosa, Paul van Mulbregt, and SciPy 1.0 Contributors. SciPy 1.0: Fundamental Algorithms for Scientific Computing in Python. *Nature Methods*, 17:261–272, 2020.

[46] Michael L. Waskom. seaborn: statistical data visualization. *Journal of Open Source Software*, 6(60):3021, 2021.

[47] J. D. Hunter. Matplotlib: A 2d graphics environment. *Computing in Science & Engineering*, 9(3):90–95, 2007.

[48] Jacob VanderPlas, Brian Granger, Jeffrey Heer, Dominik Moritz, Kanit Wongsuphasawat, Arvind Satyanarayan, Eitan Lees, Ilia Timofeev, Ben Welsh, and Scott Sievert. Altair: Interactive statistical visualizations for python. *Journal of Open Source Software*, 3(32):1057, 2018.

[49] Arvind Satyanarayan, Dominik Moritz, Kanit Wongsuphasawat, and Jeffrey Heer. Vega-lite: A grammar of interactive graphics. *IEEE transactions on visualization and computer graphics*, 23(1):341–350, 2017.

[50] The pandas development team. pandas-dev/pandas: Pandas, February 2020.

[51] Wes McKinney. Data Structures for Statistical Computing in Python. In Stéfan van der Walt and Jarrod Millman, editors, *Proceedings of the 9th Python in Science Conference*, pages 56 – 61, 2010.

[52] Adam Paszke, Sam Gross, Francisco Massa, Adam Lerer, James Bradbury, Gregory Chanan, Trevor Killeen, Zeming Lin, Natalia Gimelshein, Luca Antiga, Alban Desmaison, Andreas Kopf, Edward Yang, Zachary DeVito, Martin Raison, Alykhan Tejani, Sasank Chilamkurthy, Benoit Steiner, Lu Fang, Junjie Bai, and Soumith Chintala. Pytorch: An imperative style, high-performance deep learning library. In H. Wallach, H. Larochelle, A. Beygelzimer, F. d Alché-Buc, E. Fox, and R. Garnett, editors, *Advances in Neural Information Processing Systems 32*, pages 8024–8035. Curran Associates, Inc., 2019.

[53] Thomas Kluyver, Benjamin Ragan-Kelley, Fernando Pérez, Brian Granger, Matthias Bussonnier, Jonathan Frederic, Kyle Kelley, Jessica Hamrick, Jason Grout, Sylvain Corlay, Paul Ivanov, Damián Avila, Safia Abdalla, Carol Willing, and Jupyter development team. Jupyter notebooks - a publishing format for reproducible computational workflows. In Fernando Loizides and Birgit Scmidt, editors, *Positioning and Power in Academic Publishing: Players, Agents and Agendas*, pages 87–90, Netherlands, 2016. IOS Press.

[54] A F M Smith and A E Gelfand. Bayesian statistics without tears: A Sampling-Resampling perspective. *Am. Stat.*, 46(2):84–88, 1992.

[55] Kevin P Murphy. *Machine learning: a probabilistic perspective*. MIT press, 2012.

[56] Arthur Gretton, Karsten M Borgwardt, Malte J Rasch, Bernhard Schölkopf, and Alexander Smola. A kernel two-sample test. *The Journal of Machine Learning Research*, 13(1):723–773, 2012.

[57] Aaditya Ramdas, Sashank Jakkam Reddi, Barnabás Póczos, Aarti Singh, and Larry Wasserman. On the decreasing power of kernel and distance based nonparametric hypothesis tests in high dimensions. In *Proceedings of the AAAI Conference on Artificial Intelligence*, volume 29, 2015.

[58] Bharath K Sriperumbudur, Kenji Fukumizu, Arthur Gretton, Bernhard Schölkopf, and Gert RG Lanckriet. On integral probability metrics,\phi-divergences and binary classification. *arXiv preprint arXiv:0901.2698*, 2009.

[59] Marco Cuturi. Sinkhorn distances: Lightspeed computation of optimal transport. *Advances in neural information processing systems*, 26:2292–2300, 2013.

[60] Thejs Brinckmann and Julien Lesgourgues. MontePython 3: boosted MCMC sampler and other features. *Phys. Dark Univ.*, 24:100260, 2019.

[61] Eleonora Di Valentino et al. Exploring cosmic origins with CORE: Cosmological parameters. *JCAP*, 04:017, 2018.

[62] Laurence Perotto, Julien Lesgourgues, Steen Hannestad, Huitzu Tu, and Yvonne Y. Y. Wong. Probing cosmological parameters with the CMB: Forecasts from full Monte Carlo simulations. *JCAP*, 10:013, 2006.

[63] Jonas Degrave and Ira Korshunova. Why machine learning algorithms are hard to tune and how to fix it. `https://www.engraved.blog/why-machine-learning-algorithms-are-hard-to-tune/`, Jan 2021.

[64] John Platt and Alan Barr. Constrained differential optimization. In D Anderson, editor, *Neural Information Processing Systems*. American Institute of Physics, 1988.

A Experiments

In this section we present the relevant experimental details including a comprehensive list of experiments in Table 2. We first discuss the computational setting and approximate computational cost. Afterwards the details for the SBI benchmark, the torus, and the eggbox are presented. Finally we discuss how we generate our datasets and how we can use the estimated likelihood-to-evidence ratio in practice. In all tests, we applied TMNRE with the hyperparameters laid out in Table 3.

Table 2: Experiments

Task	Parameter Dimension	Algorithm	Simulations	Trained Marginalization	Evaluated Marginalization	Constrained	Metric
GLU	10	TMNRE	$\{1, 10, 100\}$E3	1d, 2d	1d, 2d	1d	C2ST-ddm
GLU	10	SBI	$\{1, 10, 100\}$E3	Joint	1d, 2d		C2ST-ddm
Gaussian Mixture	2	TMNRE	$\{1, 10, 100\}$E3	1d, 2d	1d, 2d	1d	C2ST-ddm
Gaussian Mixture	2	SBI	$\{1, 10, 100\}$E3	Joint	1d, 2d		C2ST-ddm
SLCP	5	TMNRE	$\{1, 10, 100\}$E3	1d, 2d	1d, 2d	1d	C2ST-ddm
SLCP	5	SBI	$\{1, 10, 100\}$E3	Joint	1d, 2d		C2ST-ddm
SLCP (distractors)	5	TMNRE	$\{1, 10, 100\}$E3	1d, 2d	1d, 2d	1d	C2ST-ddm
SLCP (distractors)	5	SBI	$\{1, 10, 100\}$E3	Joint	1d, 2d		C2ST-ddm
Two Moons	2	TMNRE	$\{1, 10, 100\}$E3	1d, 2d	1d, 2d	1d	C2ST-ddm
Two Moons	2	SBI	$\{1, 10, 100\}$E3	Joint	1d, 2d		C2ST-ddm
Torus	3	TMNRE	4985, 11322, 21127, 32032	1d, 2d	1d, 2d	1d	C2ST-ddm, KLD, Visual
Torus	3	MNRE	4985, 11322, 21127, 32032	1d, 2d	1d, 2d		C2ST-ddm, KLD, Visual
Torus (epsilon scan)	3	TMNRE	$\sim$ 30 E3	1d, 2d	1d, 2d	1d	C2ST-ddm / simulation
Egg Box 2 modes / dim	10	MNRE	10 E3	1d, 2d	1d, 2d		Visual
Egg Box 2 modes / dim	10	NRE	10 E3	Joint	1d, 2d		Visual
Egg Box 2 modes / dim	10	SNRE	10 E3	Joint	1d, 2d		Visual
Egg Box 2 modes / dim	10	SMNRE	10 E3	1d, 2d	1d, 2d		Visual

Table 3: TMNRE Hyperparameters

Hyperparameter	Value
Activation Function	RELU
AMSGRAD	No
Architecture	RESNET (2 blocks)
Batch normalization	Yes
Criterion	BCE
Dropout	No
Early stopping patience	20
Epsilon	$e^{-13} \approx 10^{-6}$
Hidden features	64
Percent validation	10%
Reduce lr factor	0.1
Reduce lr patience	5
Max epochs	300
Max rounds	10
Learning rate	0.01
Learning rate scheduling	Decay on plateau
Optimizer	ADAM
Weight Decay	0.0
Z-score observations	online
Z-score parameters	online

A.1 Total Compute

Most calculations were performed on a local computing cluster which offered ten TitanX GPU nodes. We estimate the total computation time, including prototype runs, was approximately 613 GPU hours. We calculated the cost of one run of the benchmark then multiplied it by 10 for this estimation. The computation of the C2ST-ddm on the marginals from existing data was performed on the same cluster but using cpu nodes. According to `mlco2.github.io` this would imply 66.3 kg CO_2 at a normal institution; however, our cluster is run exclusively on wind power.

Table 4: Actual bounds of stochastic simulation budget for TMNRE along with number of rounds before the stoppping criterion was reached. Maximum of one round implies that there was no truncation and the method is effectively doing MNRE.

Marginal Task	Simulation Budget	Min simulation count	Max simulation count	Min Rounds	Max Rounds
Two Moons	1000	934	1056	1	4
	10000	9941	10558	1	4
	100000	99863	104919	2	3
Gaussian Linear Uniform	1000	952	1056	1	1
	10000	9760	10469	1	4
	100000	100223	105468	1	4
SLCP	1000	949	1050	1	1
	10000	9901	10546	1	1
	100000	99616	104968	1	2
SLCP Distractors	1000	951	1035	1	1
	10000	9931	10141	1	1
	100000	99431	100882	1	1
Gaussian Mixture	1000	954	1072	1	4
	10000	9902	10582	2	4
	100000	99567	105704	2	3

A.2 SBIBM details

We performed a marginalized version of the SBI benchmark on a subset of the tasks [38], namely Two Moons, Gaussian Linear Uniform, SLCP, SLCP Distractors, and Gaussian Mixture. Each task has ten parameters drawn from the corresponding prior. Each of those parameters are pushed through the simulator and those become ten observations with a known ground truth posterior and true generating parameter.

Two Moons has a two dimensional posterior where the mass is concentrated into two separated half circles. Gaussian Linear Uniform's simulator simply takes the underlying parameter to be the mean of a ten dimensional spherical Gaussian. Therefore, the posterior is merely a Gaussian, cutoff by the uniform prior. SLCP stands for simple likelihood complex posterior and has a five dimensional parameter space which, after a nonlinear transformation, define the mean and covariance of a two-dimensional, non-spherical Gaussian. Four points are sampled from this Gaussian and that serves as the observational data. SLCP Distractors is just like SLCP but contains 92 superfluous dimensions in the data which are concatenated with the observational data from SLCP. Finally, Gaussian Mixture defines a simulator which is simply a mixture of two, two-dimensional Gaussians with the same parameterized mean but one has a much wider covariance than the other. For the exact details we refer the reader to Ref. [38] where these tasks are defined at great length. A summary of some of the details for each of these tasks, and the algorithm applied to them, are contained in the Experiment Table 2.

The other methods estimated the joint posterior in some manner while TMNRE targeted the marginals directly. The full list of alternative methods are called REJ-ABC, NLE, NPE, NRE_B, SMC-ABC, SNLE, SNPE, SNRE_B. These methods represent a significant portion of the neural simulation-based inference literature and will not be described in detail here. Please consult Ref. [38].

We defined a summary of the C2ST across the task's marginals by taking the average over same-dimensional marginals and averaged over the observations, see (9). These values are reported for all methods in Figure 1 where the 95% confidence intervals are computed for the C2ST-ddm over observations, i.e. the variance across marginals in the C2ST-ddm calculation is not carried forward into the reported uncertainty. We found it to be very small compared to the reported values and was unlikely to make a significant difference.

The authors note that data and code was used from SBIBM which can be found on GitHub at `https://github.com/sbi-benchmark/sbibm`. It is distributed with the MIT license.

Out method TMNRE was trained to learn all one and two dimensional likelihood-to-evidence ratios thereby predicting the posterior distribution. Since we applied TMNRE, the algorithm truncated the prior distribution depending on the learned marginal likelihood-to-evidence ratio. We gave a generous maximum of ten rounds but no task used so many. The maximum was four before the stopping criterion was satisfied. We used the ratio of the constrained prior mass from the current round to

the previous round, namely β in Algorithm 1, as a stopping criterion and set it to 0.8. The stopping criterion was satisfied after a certain number of rounds details about the maximum and minimum round for every task, at every budget, can be found in Table 4. We applied the heuristic for the simulation budget found in Appendix A.5.

The final estimated likelihood-to-evidence ratio approximates the posterior on the constrained region. Samples were drawn from this posterior using rejection sampling. The samples from these marginals, in the constrained region, are used for the reported C2ST-ddm in Figure 1.

A.3 Torus details

We use a simulator and prior with a torus shaped posterior to showcase three aspects of TMNRE. The ground truth can be seen on the left in Figure 2. We proceed with the details of the simulator followed but subsections which give the details for every showcase experiment.

If we let $\boldsymbol{\theta}, \boldsymbol{g}(\boldsymbol{\theta}) \in \mathbb{R}^3$ and θ_k denote the kth element of $\boldsymbol{\theta}$, then the simulator for this problem is defined $\boldsymbol{g}(\boldsymbol{\theta}) = (\theta_0, \sqrt{(\theta_0 - a)^2 + (\theta_1 - b)^2}, \theta_2)^T$. The likelihood is defined by an additive noise model, namely $p(\boldsymbol{x} \mid \boldsymbol{\theta}) = \mathcal{N}(g(\boldsymbol{\theta}), \boldsymbol{\Sigma})$ where a, b are constant scalars and $\boldsymbol{\Sigma}$ is a diagonal, positive definite matrix. In our experiments we let $a = 0.6$, $b = 0.8$, and $\boldsymbol{\Sigma} = \text{diag}(0.03^2, 0.005^2, 0.2^2)$. To ensure an approximately torus-shaped posterior, we select a "noiseless" observation of interest $\boldsymbol{x}_0 = \boldsymbol{g}(\boldsymbol{\theta}_0)$ and parameters $\boldsymbol{\theta}_0 = (0.57, 0.8, 1.0)^T$.

A.3.1 Torus TMNRE and MNRE Metrics

Since we did not have a clear simulation budget during the initial run of TMNRE, we determined the number of simulations in the following round by multiplying the retained simulations by 1.5 and sampling from a Poisson distribution. We started with 5,000 requested samples and up to 10 rounds. In the end that meant we ran Algorithm 1 with the following number of simulations in each round: 4985, 11322, 21127, 32032. The stopping criterion was met in four rounds, before the maximum number of rounds was reached.

A sample visualization of this truncation process is visible in Figure 6. As described in the text, each of these truncated priors were utilized for an ablation study where we estimated the marginal likelihood-to-evidence ratio using either the truncated prior or the true prior. In effect, testing the value of TMNRE versus MNRE. Once the number of simulations were fixed by TMNRE we used exactly the same number of simulations at that stage with MNRE.

A.3.2 Epsilon Hyperparameter Scan

To determine a useful default value for the cutoff threshold ϵ, we ran TMNRE on the torus simulator, as described above, at 10 different values of epsilon. Namely, $\epsilon_i \in \{10^i : i = -1, \ldots, -10\}$. At every round, the simulator requested approximately 10,000 more simulations than were retained from the previous round. The amount of simulations was determined stochastically, see Appendix A.5. Once the method had hit the stopping criteria, the one and two dimensional C2ST-ddm was computed and normalized by the number of simulations required to generate it. The results were plotted by truncation cutoff ϵ on the right in Figure 2. We determined that 10^{-6} minimized the C2ST-ddm approximately as well as the global minima 10^{-4} while truncating the prior more conservatively.

A.3.3 Empirical Self-Consistency Test

When we do not have a ground truth to compare to, it is important that we can determine whether the nominal credible intervals correspond to the true credible intervals. We propose to do so by comparing the nominal credibility to the empirical credibility. An explanation of how to calculate this performance metric is provided in Appendix B.3.

A.4 Eggbox details

The eggbox task is well described in the main text. The hyperparameters for NRE, SNRE, and SMNRE are all the defaults as determined by SBI [42]. We implemented SMNRE by creating a custom version of the simulator. We revealed the one or two parameters which were learned sequentially to the SMNRE algorithm while we "baked-in" the uniform prior for the other dimensions, i.e. the simulator

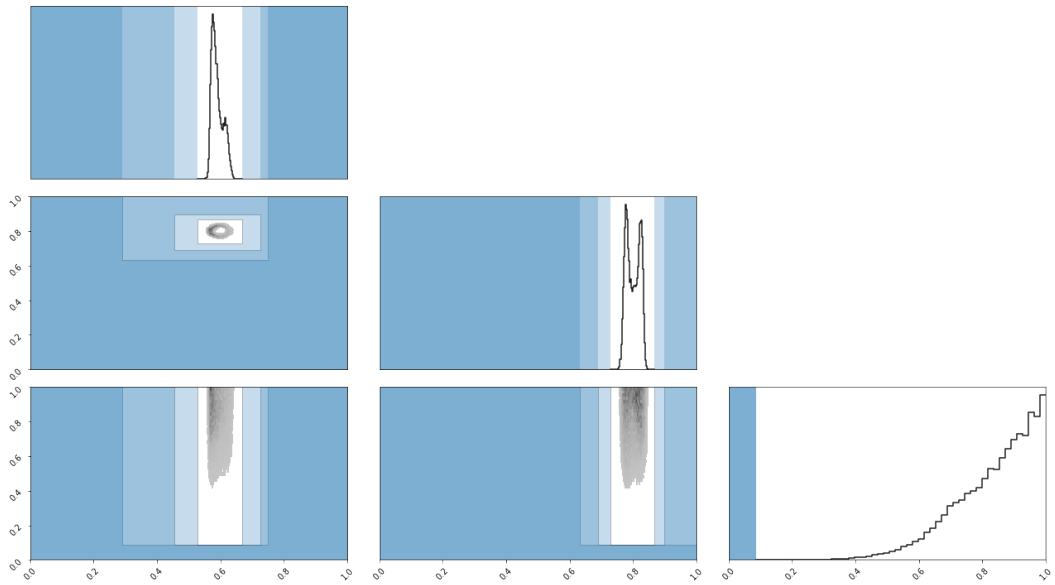

Figure 6: An example of what the truncation process looks like in both one and two dimensions. At each round, the truncated region of the indicator function is denoted in blue. The region is slightly transparent so that the evolution over rounds can be discerned. This plot helps visualize that truncation only occurs at very, very low posterior density. The entire prior region is shown to emphasize that naive sampling results in few samples within the region of interest.

sampled from a uniform distribution and simulates a concatenation of the sequentially predicted dimensions with the uniformly predicted dimensions. We expect that SMNRE fails due to its very limited number of simulations. This limitation might seem pathological in this symmetric setting but it is very real in a simulator which defines an unknown posterior that may or may not have symmetry.

A.5 Simulation budget and dataset generation

First, we show that it is possible to accomplish Algorithm 1 without having to sample new independently drawn parameters by pairing simulations with other parameters. Like several other algorithms [8, 14], we assure the independence of $\boldsymbol{x}$ and $\boldsymbol{\theta}$ by sampling two mini-batches from the dataset and switching the $\boldsymbol{\theta}$ parameters. This produces a pair of independently drawn parameters and simulations which can be used to calculate the loss function efficiently without sampling.

Second, we discuss our heuristic for producing a useful amount of samples within the constrained region. We divided the simulation budget between constraining and inference on the constrained region. During the constraining phase, we set the training data per round $N^{(m)} = 0.3\,B$ where B represents the entire simulation budget. This does not imply that each round used a third of the simulation budget, rather the new simulations plus the retained simulations equal a third of the budget. Finally, once the stopping criterion was satisfied, we used the remaining budget within the estimated $\hat{\Gamma}^{\text{rec}}$. We found that this technique created enough simulations during the truncation rounds to estimate Γ^{rec} relatively well while leaving a sizable portion of the simulation budget to be sampled from the truncated prior. Naturally, we want to sample as much from the truncated prior as possible to reduce simulations in regions of nearly zero probability density and increase simulator efficiency.

In contrast, sequential methods usually divide their simulation budget evenly across rounds. However, since they do not have a stopping criteria it is natural to divide the simulations that way. We used this technique when training sequential methods.

Third, we discuss the stochastic nature of our sampling technique. Rather than sampling an exact number of parameters and corresponding simulations, we instead sampled from a Poisson distribution centered at the the requested number of samples. In practice, this meant around a 5% difference between the extrema of the actual number of produced simulations and the requested number of simulations.

A.6 How do we use the likelihood-to-evidence ratio?

Histograms. Domain scientists, in particularly astronomers and astrophysicists, typically consider a visualization of the posterior and draw conclusions based on their problem-specific intuition and the reported uncertainty bounds. By learning the relevant one and two dimensional marginal likelihood-to-evidence ratios, our method can generate a visualization of the posterior, namely a corner plot of weighted histograms, by sampling from the prior $\boldsymbol{\vartheta} \sim p(\boldsymbol{\vartheta})$ and sorting the results into bins. Each sample's contribution is weighted according to the learned $\hat{r}(\boldsymbol{x} \mid \boldsymbol{\vartheta})$, creating a posterior histogram.

The histogram facilitates the computation of credible regions. In particular, finding an accurate estimate of the $(100 - \alpha)\%$ highest density credible region is the primary goal of most astronomers.

Rejection sampling. We can use our unnormalized point-wise posterior estimate as the target and the constrained prior as the proposal to generate samples distributed like the posterior via rejection sampling. Let $\tilde{p}_\Gamma(\boldsymbol{\vartheta} \mid \boldsymbol{x}) = \hat{r}_\Gamma(\boldsymbol{x} \mid \boldsymbol{\vartheta}) \mathbb{1}_\Gamma(\boldsymbol{\vartheta}) p(\boldsymbol{\vartheta})$ be our target distribution and $q(\boldsymbol{\vartheta}) = \mathbb{1}_\Gamma(\boldsymbol{\vartheta}) p(\boldsymbol{\vartheta})$ be our proposal distribution. $\mathbb{1}_\Gamma$ denotes an indicator function which is nonzero in constrained region Γ, $\tilde{p}_\Gamma(\boldsymbol{\vartheta} \mid \boldsymbol{x})$ is the unnormalized posterior, and $\hat{r}_\Gamma$ is the constrained likelihood-to-evidence ratio. Following a modified version of Maximum Likelihood Estimate (MLE)-based rejection sampling [54], we set $M = \hat{r}_\Gamma(\boldsymbol{x} \mid \hat{\boldsymbol{\vartheta}})$ where $\hat{\boldsymbol{\vartheta}} = \arg\max_{\boldsymbol{\vartheta}} \hat{r}_\Gamma(\boldsymbol{x} \mid \boldsymbol{\vartheta})$ is the MLE. We sample parameters from the proposal distribution $\boldsymbol{\vartheta} \sim q(\boldsymbol{\vartheta})$ and accept them with probability $\frac{\tilde{p}_\Gamma(\boldsymbol{\vartheta}|\boldsymbol{x})}{Mq(\boldsymbol{\vartheta})} = \frac{\hat{r}_\Gamma(\boldsymbol{x}|\boldsymbol{\vartheta})}{\hat{r}_\Gamma(\boldsymbol{x}|\hat{\boldsymbol{\vartheta}})}$.

The acceptance probability is tolerable when the parameter space is low dimensional and the constrained prior is not significantly wider than the posterior [55]. For our method, the first condition generally holds but the second is not guaranteed. Despite this potential inefficiency, the parallel proposal and rejection of samples is resolved quickly when the acceptance probability is not vanishingly small. In that case, likelihood-free MCMC [8, 14, 38] becomes unavoidable.

B Evaluation metrics

We introduce here the relevant evaluation metrics that we will use for our below experiments. These are relevant both to compare our results with the ground-truth (C2ST, KL divergence), as well as for studying desirable statistical properties of the posterior without requiring knowledge of the ground-truth (coverage testing). Here, C2ST is motivated by its omnipresence in the simulator-based inference literature, to which we want to compare. We additionally introduce KL divergence as a metric that is tractable for the low-dimensional marginal posteriors that are the focus of this paper.

The neural likelihood-free inference reports several performance metrics which do not apply well to our method... Reporting $-\mathbb{E}[\log q(\boldsymbol{\theta}_o \mid \boldsymbol{x}_o)]$ is quite common throughout the literature [8, 10–12, 14]. Since we learn an unnormalized posterior, we cannot compare our value to other methods. Furthermore it is a poor indicator of performance [38]. Another common technique is to measure the median distance between posterior-predictive samples [10, 11, 14] but this is impossible since we learn a marginalized posterior and cannot sample from the posterior predictive distribution. Maximum Mean Discrepancy (MMD) [56, 57] has been found to be sensitive to choice of hyperparameters [38]. It is in principle possible to apply other alternatives such at the Wasserstein distance [58] using the Sinkhorn-Knopp algorithm [59] but there is not literature precedent.

B.1 Kullback–Leibler Divergence

Since this paper is primarily interested in determining low dimensional marginal posteriors, it is feasible to estimate the Kullback–Leibler divergence, denoted D_{KL}, using samples and comparing the histograms. We've found that this method for approximating the Kullback–Leibler divergence is hyperparameter dependent, namely based off the number of bins. We only reported the Kullback–Leibler divergence for the torus problem and we used 100 bins. This effect implies that only the difference between Kullback–Leibler divergences is relevant.

B.2 Classifier 2-Sample Test per d-Dimensional Marginal (C2ST-ddm)

The classifier 2-sample test (C2ST) [39, 40] is a performance metric where a classifier is trained to differentiate between samples from the ground truth and approximate posterior. It features an

interpretable scale where 1.0 implies that the classifier could distinguish every pair of samples the distributions while 0.5 implies indistinguishably. It is possible to determine where distributions differ using this metric [38].

We define the *C2ST per d-Dimensional Marginal (C2ST-ddm)* test statistic, which reports the average C2ST across every pair of d-dimensional marginals. Consider two random variables $\boldsymbol{X} \sim P(\boldsymbol{X}), \boldsymbol{Y} \sim Q(\boldsymbol{Y})$ with $\boldsymbol{X}, \boldsymbol{Y} \in \mathbb{R}^D$ and hyperparameter $1 \leq d \leq D$ that represents the marginal dimensionality of interest. Let $(S_P, S_Q) \coloneqq \left\{(S_{P_k}, S_{Q_k}) : k \in \{1, 2, \ldots, \binom{D}{d}\right\}$ where $S_{P_k} \coloneqq \{\boldsymbol{x}_k^{(1)}, \ldots, \boldsymbol{x}_k^{(n)}\} \sim P(\boldsymbol{X}_k)$ and $S_{Q_k} \coloneqq \{\boldsymbol{y}_k^{(1)}, \ldots, \boldsymbol{y}_k^{(n)}\} \sim Q(\boldsymbol{Y}_k)$ are sets of n samples drawn from the kth d-dimensional marginal of P and Q, respectively. Now,

$$\text{C2ST-ddm}(S_P, S_Q) \coloneqq \frac{1}{K} \sum_{k=1}^{K} \text{C2ST}\left(S_{P_k}, S_{Q_k}\right), \text{ with } K = \binom{D}{d}. \tag{9}$$

For our problem, we let $P_k = p(\boldsymbol{\vartheta}_k \mid \boldsymbol{x}_o)$ and $Q_k = \hat{r}_k(\boldsymbol{x}_o \mid \boldsymbol{\vartheta}_k) p(\boldsymbol{\vartheta}_k)$.

B.3 Empirical Credible Interval Testing

Evaluating the accuracy of a posterior approximation requires access to the ground-truth and the ability to compute a suitable metric or divergence. While acceptable during benchmarking [38], this is impossible for practitioners because they only have access to the observation $\boldsymbol{x}_o$. Domain scientists depend on sanity checks such as coverage testing and comparison between estimation methods to verify that the reported posterior is accurate. Coverage testing is designed for frequentist confidence intervals; however, we apply a similar technique to test the validity of our credible intervals, empirically.

We report a nominal (100 - α)% credible region but the effects of approximation or training might have influenced the contour's shape. Our empirical testing checks whether the nominal contour aligns with the contour ground truth by considering many realizations of $\boldsymbol{x}$ and dividing the number of times the corresponding $\boldsymbol{\theta}$ falls within the nominal credible region by the number of $(\boldsymbol{\theta}, \boldsymbol{x})$s that were tested. When this is the case, the blue line and the orange line intersect in visualizations like Figure 4.

One major advantage of an amortized method for a real-world practitioner is the possibility of quickly performing tests like these. During the training process many parameter-simulation pairs have already been generated, we can use them to check the credible intervals of our method. Note that sequential methods cannot do this without great expense because they would have to retrain their posterior estimator on every tested observation.

C Comparing the truncated marginal likelihood-to-evidence ratio to the truth

C.1 Exemplary error estimates

We will consider the effect of truncation on a multivariate normal distribution, and discuss various limiting cases. Let us assume that the true posterior has the shape of a multivariate normal distribution with mean zero and covariance matrix Σ,

$$p(\boldsymbol{\vartheta}|\boldsymbol{x}_o) = \mathcal{N}(\boldsymbol{\vartheta}|0, \Sigma) \,. \tag{10}$$

This implies that the posterior-to-maximum posterior ratio is given by

$$\frac{p(\boldsymbol{\vartheta}|\boldsymbol{x}_o)}{\max_{\boldsymbol{\vartheta}} p(\boldsymbol{\vartheta}|\boldsymbol{x}_o)} = \exp\left(-\frac{1}{2}\boldsymbol{\vartheta}^T \Sigma^{-1} \boldsymbol{\vartheta}\right) \,, \tag{11}$$

and that the same ratio for all one-dimensional marginal posteriors is given by

$$\frac{p(\theta_i|\boldsymbol{x}_o)}{\max_{\theta_i} p(\theta_i|\boldsymbol{x}_o)} = \exp\left(-\frac{1}{2}\frac{\theta_i^2}{\Sigma_{ii}}\right) \,. \tag{12}$$

Let us consider an indicator function $\mathbb{1}_\Gamma$ where Γ is defined as in Eq. (6), given some small ϵ. In the case of vanishing parameter correlations, the covariance matrix Σ is diagonal, and the posterior

factorizes like $p(\boldsymbol{\vartheta}|\boldsymbol{x}_o) = \prod_i p(\theta_i|\boldsymbol{x}_o)$. The truncation procedure can then be considered for each of the one-dimensional marginal posteriors separately: Only parameter regions where $|\theta_i| < \sqrt{-2\Sigma_{ii}\ln\epsilon}$ for all i are included in Σ. In this case ϵ directly determines how far into the tails posteriors are correctly reconstructed. Using the error function, one can show that the amount of mass that is removed by the truncation is $\epsilon/\sqrt{-\ln\epsilon}$. This motivates our general estimate of an $\mathcal{O}(\epsilon)\max_{\theta_i} p(\theta_i|\boldsymbol{x}_o)$ effect on the truncated posteriors, where the second factor is accounting for the right dimensionality of the expression.

Let us consider the opposite extreme of a maximally correlated posterior, with a covariance matrix that is given by $\Sigma_{ii} = 1$ and $\Sigma_{ij} = 1 - \xi$ for $i \neq j$, and where $\xi \ll 1$. Again, marginal posteriors are given by Eq. (12). Since the support of the maximally correlated posterior is essentially focused on the line $\theta_1 \simeq \theta_2 \simeq \cdots \simeq \theta_d$, truncations in all directions are identical. As a result, marginal posteriors are affected exactly as in the previous diagonal case.

Finally, let us consider a mildly correlated posterior in two dimensions. In this case, the region Γ would be again identified through $|\theta_i| < \sqrt{-2\Sigma_{ii}\ln\epsilon}$ for $i = 1, 2$, but since the posterior does not factorize anymore integrals on the constrained region become non-trivial. However, since only $\mathcal{O}(\epsilon)$ of posterior mass lies outside of Γ, this implies that only a similarly small mass fraction can be re-distributed in the truncated marginal posteriors $p_\Gamma(\theta_i|\boldsymbol{x}_o)$. This can significantly affect the far low-mass tails of the distribution, with negligible effect on the high mass density regions of the posterior.

C.2 A general estimate

Let us consider an indicator function defined through Eq. (8), first for a single marginal θ_i. The removed probability mass is then given by

$$\delta M_\epsilon = \int_{\Omega_i} d\theta_i p(\theta_i|\boldsymbol{x}_o)\,\mathbb{1}\left[p(\theta_i|\boldsymbol{x}_o) < \epsilon \max_{\theta_i} p(\theta_i|\boldsymbol{x}_o)\right] ,$$

where $\mathbb{1}$ denotes an indicator function. An upper bound on the removed probability mass is then given by

$$\delta M_\epsilon < \epsilon \max_{\theta_i} p(\theta_i|\boldsymbol{x}_o) \int_{\Omega_i} d\theta_i\,\mathbb{1}\left[p(\theta_i|\boldsymbol{x}_o) < \epsilon \max_{\theta_i} p(\theta_i|\boldsymbol{x}_o)\right] ,$$

For a compact Ω_i, this leads to the claimed bound in one dimension. However, also in the case of a larger number of parameters, each truncation would remove at most mass at the level of $\mathcal{O}(\epsilon)$, leading to an overall $\mathcal{O}(\epsilon)$ effect on the estimated posteriors. We emphasize that in the case of priors with non-compact support, a re-parametrization onto priors with compact support can lead to smaller coefficients in front of ϵ.

D Limitations

We note two kinds of limitations: First, we address limitations when the method works as planned. Second, we address failure modes.

When the posterior distribution is nearly as wide as the prior, we do not gain much by truncating the prior distribution. In this case our method would reduce to MNRE. However, this is rarely the case in physics where the paradigm is to define an uninformative prior distribution across the accepted bounds for a parameter and the posterior will be contained in fractions of that prior's mass.

Another limitation is that the truncation by hyperrectangle is inherently inefficient when the marginals of interest are highly correlated. In that situation, we are interested in a hyperellipse within the constrained hyperrectangle but our current formulation cannot utilize this heuristic. This problem possible to solve by using techniques from Nested Sampling which regularly seeks to efficiently sample from within a certain density contour.

The failure modes are perhaps more obvious. If our initial round of sampling is too sparse, it is possible to incorrectly "miss' a region of high posterior density and cut it out of our analysis. If the initial region is satisfactorily sampled from, this will not occur.

Another failure mode is related to the local amortization that our ratio estimators learn. While they are able to estimate any posterior from a parameter drawn within the truncated prior, it may be that some

of the posterior runs into the truncation. This can be identified whenever a posterior equicontour line intersects with the truncation bounds. In general, we suggest limiting the use of the locally amortized predictions to ones closer to the ground truth generating parameter than to the truncation bounds.

E Performance on physics example

Parameter inference plays a important role in modern cosmology. Here we use a simulator that takes six parameters (specifying the underlying ΛCDM cosmological model) and returns three lensed angular power spectra $C_\ell^{TT}, C_\ell^{TE}, C_\ell^{EE}$ (where T denotes temperature and $E =$ denotes E-mode polarization) as they would be measured by an idealized Cosmic Microwave Background (CMB) experiment. The likelihood-based approach to inference in this context is provided by popular packages such as `MontePython` [60]. Our simulator is identical to the likelihood that in `MontePython` is called `fake_planck_realistic` [61]. This likelihood is used, often in combination with other likelihoods, to forecast the expected constraining power of future experiments. In this model, the power spectra receive non-stochastic contributions from the cosmological model and the idealized measurement instrument. Stochasticity is implemented in the form of *cosmic variance*, which reflects the fact that for fixed ℓ, each C_ℓ is determined by measuring $2\ell + 1$ modes in the sky. The result is that the collection of C_ℓ obeys a Wishart distribution, which at large ℓ can be approximated as a multivariate normal distribution. For more details see [62]. Draws from the simulator with and without noise are shown in Fig. 7.

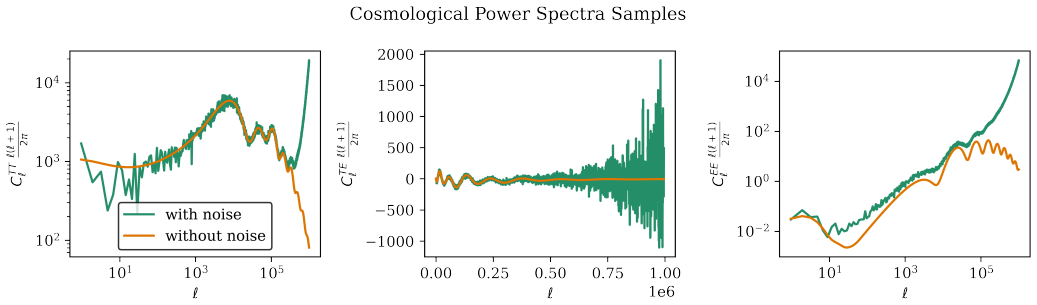

Figure 7: A sample drawn from the CMB simulator, with the cosmological contribution in orange and the noise-added sample in green. The noise model amounts to a non-stochastic contribution from the instrument as well as a stochastic contribution (following a Wishart distribution) corresponding to cosmic variance, in other words the fact that an individual C_ℓ is determined by measuring $2\ell + 1$ modes.

We use this example to study the utility of *marginal* ratio estimation. As such, we do not use multiple rounds of simulation and training. This is in part due to the availability of a tractable likelihood, which allows us to perform a Fisher estimation (i.e. Gaussian approximation) of the expected marginal probability contours. Although the ground-truth posteriors for this inference problem turn out to be slightly non-Gaussian, the Fisher estimation suffices to derive a reasonable region in parameter space for inference. We therefore take a uniform prior with $\theta_d \in \left[\overline{\theta}_d - 5\sigma_d^F, \overline{\theta}_d + 5\sigma_d^F\right]$, where $\overline{\theta}_d$ denotes the ground truth parameter value and $\sigma_d^F = \sqrt{(F^{-1})_{ii}}$ is the Fisher estimation of the 1σ region for parameter i.

We compare three approaches with 5,000 samples. For comparison, an MCMC analysis of this problem converges after roughly 45,000 accepted samples with an acceptance rate of ~ 0.3. We compare TMNRE, NRE, and MCMC with a limited number of samples. For MCMC we use a pre-computed covariance matrix for proposal steps, determined by running a chain until convergence. For inference with TMNRE and NRE, we use a linear compression layer that takes the concatenated power spectra (each with $\ell \in [2, 2500]$, so that the full data vector has 7497 entries) and outputs 10 features. The same linear compression network is shared between different ratio estimators. In other words, we introduce a shared feature embedding of the data such that the entire neural network has the form

$$f_{\phi,k}(\boldsymbol{x}, \boldsymbol{\vartheta}_k) = g_{\phi_g,k}(\boldsymbol{F}_{\phi_{\boldsymbol{F}}}(\boldsymbol{x}), \boldsymbol{\vartheta}_k) \tag{13}$$

where $\boldsymbol{F}$ is the feature embedding, k represents the index of the marginal-of-interest, g is an MLP, and ϕ represents the network weights from both g and f. This is appealing computationally but, unlike with ϕ_g, the weights of the feature embedding are dependent on the loss of every marginal. This is the multi-target training paradigm and can be difficult to tune [63, 64]; however, this is not a problem for us in practice. The hyperparameters are written in Table 5.

The results are shown in Fig. 8. We see that TMNRE reproduces the ground-truth 1- and 2-σ contours very accurately. On the other hand, NREresults in hardly any constraint on the parameter space, while the limited MCMC run does not have accurate 2-σ contours.

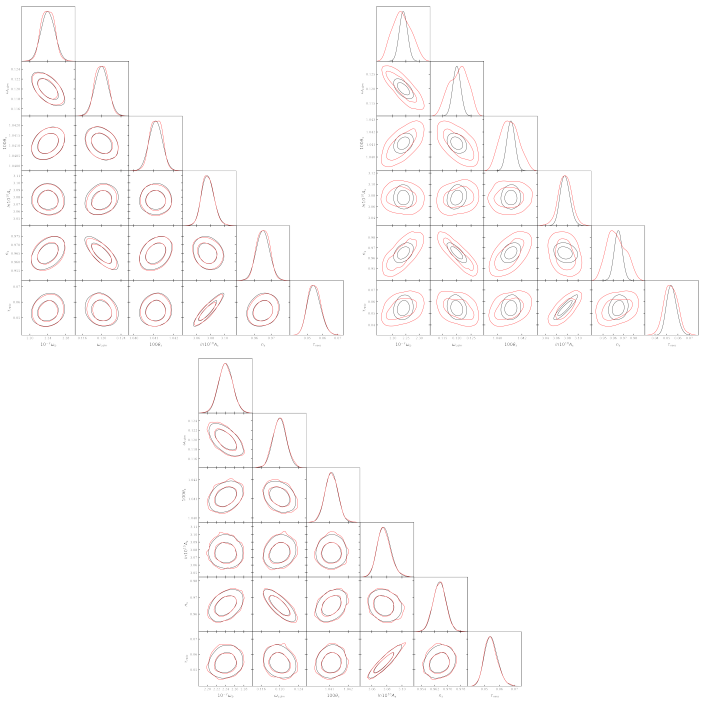

Figure 8: Corner plots for various methods using 5,000 simulations (in red) vs. ground-truth MCMC (45,000 accepted samples with acceptance rate ~ 0.3, in black). Left: results for TMNRE. We see excellent agreement with the ground truth. Center: corner plot for NRE. With 5,000 samples, the marginal posteriors are hardly constrained. Right: corner plot for MCMC with 5,000 accepted (burn-in removed) samples vs. converged MCMC chain. While the short chain gives accurate 1σ contours, it does not yield accurate for the 2σ contours.

Table 5: Physics Example Hyperparameters

Hyperparameter	Value
Activation Function	Feature Embedding: None, Ratio Estimator: RELU
AMSGRAD	No
Architecture	Feature Embedding: One Linear Layer, Ratio Estimator: MLP
Batch normalization	No
Criterion	BCE
Dropout	No
Early stopping patience	5
Epsilon	N/A
Hidden features	256
Percent validation	10%
Reduce lr factor	0.25
Reduce lr patience	2
Max epochs	300
Max rounds	N/A
Learning rate	0.001
Learning rate scheduling	Decay on plateau
Optimizer	ADAM
Weight Decay	0.0
Z-score observations	online
Z-score parameters	online